Energetics of Nonlinear Geostrophic Adjustment*

EMMANUEL BOSS AND LUANNE THOMPSON

School of Oceanography, University of Washington, Seattle, Washington

31 May 1994 and 20 September 1994

ABSTRACT

Solutions and energetics for nonlinear geostrophic adjustment with an initial height perturbation of the order of the total fluid depth are computed and compared to solutions derived assuming linear dynamics. Both axisymmetric and zonally uniform profiles in 1 1/2- and 2-layer shallow-water models are considered. Nonlinearities are present due to the finite perturbation in the initial depth and the nonzero centripetal acceleration. The comparison yields differences in both the magnitude and the partition of energy. In the adjusted state of a zonally uniform step, the total energy of the linear solution is a very good approximation to, and is slightly less than, the total energy of the nonlinear solution. Less resemblance is found for a horizontally bounded perturbation where for a positive (negative) perturbation in initial depth, the nonlinear final state has more (less) energy than the linear one. Addition of a second layer increases the contrast between the linear and nonlinear solutions, especially when one of the layers is shallow. In all the adjustment problems considered, the ratio of the adjusted state kinetic energy to the potential energy released during the adjustment is smaller than or equal to 1/3. A simple model describing the adjustment of a convective chimney illustrates the dependence of its energetics on initial radius and depth. The available potential energy of its adjusted state is important because it determines the growth rate of baroclinic instability.

1. Introduction

Since Rossby (1937) first studied the adjustment of a rotating fluid under the influence of gravity, many studies of geostrophic adjustment have been performed (for a review see Blumen 1972 and Gill 1982). In recent years, interest in the problem has concentrated on adjustment in fronts (Ou 1984; van Heijst 1985), penetrative convection (Killworth 1992; Hermann and Owens 1993), and eddies (McWilliams 1988; Dewar and Killworth 1990). In these studies the final (adjusted) state of the fluid is computed using its initial state and conservation principles such as potential vorticity (PV) and mass.

Gill (1976, 1982) studied the evolution of a fluid with an initial zonal step in the surface elevation. Linearizing for small perturbations, he calculated both the initial transient and the final steady solution. He showed that the energy lost during the adjustment is radiated away as inertia–gravity waves. Hermann and Owens (1993, hereafter HO) have analyzed a similar problem with an axisymmetric initial height anomaly. Middleton (1987) calculated the energetics of the adjustment of a linear zonally uniform and an axisymmetric initial height perturbation as a function of the initial perturbation spectrum. He hypothesized that the linear results obtained should pertain to the nonlinear adjustment of multilayered fluids. Since superposition is not applicable to nonlinear solutions, assessment of Middleton's hypothesis has to be done on a case by case analysis. The first step to testing this hypothesis is to look at the adjustments of finite height perturbations, which we present here.

While the adjusted state of a linearized adjustment problem depends solely on the initial PV distribution, the final state of the nonlinear problem depends on both initial mass and momentum distributions. That is, the source of the anomaly in PV is important. In order to compare our results with previous studies, we concentrate on adjustments in which the initial height field is piecewise constant and the fluid is initially at rest. The adjusted state is computed assuming conservation of mass and PV for a hydrostatic, inviscid, and Boussinesq shallow-water fluid. We revisit both Gill's (1976) and HO's adjustments, allowing for order-one height perturbation and centripetal acceleration.

An oceanic example of this problem is the geostrophic adjustment of a convective chimney. The mass field is set by convection and then relaxes under gravity (for a review see Killworth 1979, HO; and references therein). Killworth (1992) studied the collapse of a cylinder imbedded in an infinite layer (i.e., a 1 1/2-layer model) in connection with convective chimney collapse. Dewar and Killworth (1990) analyzed the same

* University of Washington School of Oceanography Contribution Number 2128.

Corresponding author address: Emmanuel Boss, School of Oceanography, Box 357940, University of Washington, Seattle, WA 98195. E-mail: boss@ocean.washington.edu

problem in a 2-layer fluid. In both studies, the nonlinear terms in the momentum and mass equations were retained. HO used both an analytic 1½-layer linear adjustment model and a three-dimensional continuously stratified nonlinear numerical model to study the spreading and collapse of chimneys.

We extend the analytical models discussed above by allowing the cylinder to be connected to a deeper (finite) layer of fluid. This configuration is supported by observations of convective chimneys (Anati and Stommel 1970; Gascard 1978; Leaman and Schott 1991). We emphasize the energetics of the chimney's adjustment since its available potential energy (APE) is the source of energy that could be converted, through baroclinic instability, into smaller-scale geostrophic motions. The growth rate of the instability is proportional to the square root of the APE (HO and references therein) and determines how soon the instability will cause the break up of the chimney. This energy may be reduced if a faster (than the instability) geostrophic adjustment takes place.

In section 2, we revisit Gill's adjustment problem, solving for the nonlinearly adjusted final state of an initial step in both 1½- and 2-layer shallow-water models. In section 3, we study the adjustment of an axisymmetric finite perturbation. Allowing for both positive and negative height perturbations, we compare our results to the results previously obtained for the linear model (HO). In section 4, we introduce a simple model of a convective chimney. This is a special case of a more general model of a 2-layer axisymmetric adjustment derived in the appendix. In section 5, we present the conclusions.

2. Infinite step adjustment

a. The 1½-layer model

We first consider the adjustment of a step perturbation in a 1½-layer shallow-water model (Fig. 1 with $h_1 \to \infty$). The linear version is found in Gill (1982, chapter 7.2). The lower layer is initially at rest, with initial height (H_2) given by

$$H_2 = \begin{cases} H_{21}, & y < 0 \\ H_{22}, & y > 0, \end{cases} \tag{1}$$

with y positive to the north. After adjustment, PV conservation and geostrophy give

$$\frac{f}{H_{2k}} = \frac{f - u_{2y}}{h_2} \tag{2}$$

$$fu_2 = -g'h_{2y}, \tag{3}$$

where $k = 1, 2$ with 1 denoting the south side of the PV front, u the alongfont velocity, g' the reduced gravity, and f the Coriolis parameter. The subscript y denotes differentiation ($\partial\cdot/\partial y$). Combining these yields a second-order ordinary differential equation (ODE) for u_2:

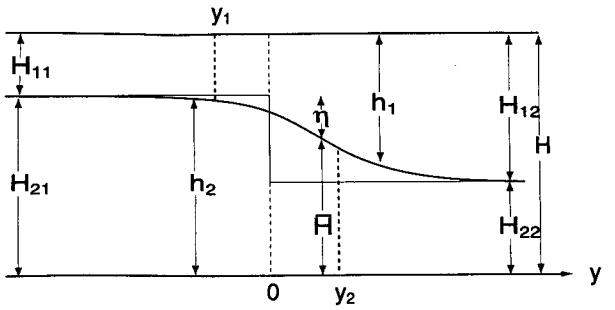

FIG. 1. Schematic for the adjustment of a zonally uniform 2-layer step. The initial state (thin line) and the adjusted state (solid line). The broken lines at y_1 and y_2 denote the locations of the PV fronts after the adjustment (initially they are at 0), $\bar{H}$ denotes the arithmetic mean of the lower-layer depth, η the deviation of the initial state from the mean, H_{ik} the initial depth of layer i at side k, h_i the adjusted depth of layer i, and H the total fluid depth. Notice that for both layers the PV front moves towards the shallower water.

$$u_{2yy} - \frac{f^2}{H_{2k}g'}u_2 = 0. \tag{4}$$

Denoting the position of the PV front as y_2, and requiring that the velocity be continuous there, the solution of (4) is

$$u_2 = \begin{cases} Ae^{(y-y_2)/\lambda_{21}}, & y < y_2 \\ Ae^{-(y-y_2)/\lambda_{22}}, & y > y_2, \end{cases} \quad \text{with} \quad \lambda_{2k} = \frac{\sqrt{g'H_{2k}}}{f}. \tag{5}$$

Using (2) and (5), the height profile is given by

$$h_2 = \begin{cases} H_{21} - \left(\dfrac{H_{21}}{g'}\right)^{1/2} Ae^{(y-y_2)/\lambda_{21}}, & y < y_2 \\ H_{22} + \left(\dfrac{H_{22}}{g'}\right)^{1/2} Ae^{-(y-y_2)/\lambda_{22}}, & y > y_2. \end{cases} \tag{6}$$

By continuity $A = \sqrt{g'}(\sqrt{H_{21}} - \sqrt{H_{22}})$ is the maximum velocity. Using mass conservation:

$$\int_{-\infty}^{0} H_{21}\,dy = \int_{-\infty}^{y_2} h_2\,dy \tag{7}$$

the PV front position (y_2) is

$$y_2 = \lambda_{21} - \lambda_{22}, \tag{8}$$

the difference between the Rossby radii on either side of the front. The shift in the position of the PV front is in the direction of the smaller initial height and increases with the perturbation. The shift of the PV front and the resulting asymmetric height and velocity fields is also seen in previous studies of nonlinear geostrophic adjustments (Rossby 1937; Blumen 1967) in which an initial momentum field was assumed.

To compare to results obtained for the linearized adjustment we define the perturbation height $\eta \equiv (H_{21}$

$- H_{22})/2$, the mean height $\bar{H} \equiv (H_{21} + H_{22})/2$, and the mean Rossby radius $\bar{\lambda} \equiv \sqrt{g'\bar{H}}/f$. The maximum velocity of the linear jet is $g'\eta/f\bar{\lambda}$, always smaller than the nonlinear one. The kinetic energy (KE) of the adjusted state and the potential energy (PE) released during the adjustment per unit length (ΔPE) are

$$\text{KE} \equiv \frac{\rho}{2}\int_{-\infty}^{\infty} h_2 u_2^2 dy = B\frac{\rho g'\bar{\lambda}\eta^2}{2},$$

$$\text{where} \quad B = \frac{2(2\bar{\lambda}^2 + \lambda_{21}\lambda_{22})}{3\bar{\lambda}(\lambda_{21} + \lambda_{22})}, \tag{9}$$

$$\Delta\text{PE} \equiv \text{PE}_{\text{initial}} - \text{PE}_{\text{adjusted}} = \frac{\rho g'}{2}\int_{-\infty}^{\infty}\{(H_2 - \bar{H})^2 - (h_2 - \bar{H})^2\}dy = 3\text{KE}. \tag{10}$$

The energy of the linearized problem is recovered in the limit of small height perturbation ($\eta \to 0$), which gives $B = 1$. For any height perturbation, B is always smaller than unity ($2\bar{\lambda} \geq \lambda_{21} + \lambda_{22}$); that is, the KE of the nonlinear case is smaller than that of the linear. This change is at most a few percent (B is greater than 0.94 for the biggest perturbation, $\eta = \bar{H}$), making the linearized KE a very good approximation to the nonlinear KE for all values of η. On the other hand, in the nonlinear case less energy is released during the adjustment, so that the *total* energy of the final state (TE) is bigger than that of the linear case:

$$\text{TE}_{\text{nonlinear}} - \text{TE}_{\text{linear}} = 2(1 - B)\text{KE}_{\text{linear}} \geq 0. \tag{11}$$

This effect is once again not larger than a few percent.

Even though the nonlinear maximum velocity is greater than the linear ($= g'\eta/f\bar{\lambda}$), its average decay scale [$(\lambda_{21} + \lambda_{22})/2$] is smaller than the linear scale ($\bar{\lambda}$) and so is its height at the jet maximum so that both the KE and ΔPE of the nonlinear solution are smaller than the linear. Note that the differences in the Rossby radii result in the average PV of the linear jet being greater than the nonlinear jet.

In both linear and nonlinear adjustments, the ratio of the KE of the adjusted state to the PE released during the adjustment is constant and equals 1/3. This ratio has been found in previous studies of step-function adjustments (see Middleton 1987 and references therein).

b. The 2-layer model

We next analyze the adjustment of a step function in a fluid with two layers of finite depth (see Fig. 1 for initial conditions). The linear adjustment solution is the same as for the 1½-layer fluid (Gill 1982, p. 194) with the following changes: (i) the velocity solution [Gill's (7.2.24)] is now the solution for the shear ($u_1 - u_2$) and (ii) the height scale (e.g., in the Rossby radius) is the internal height [$H_1H_2/(H_1 + H_2)$, where H_i is the mean depth of the ith layer]. The absolute velocity in each layer is found by requiring that there be no barotropic transport. The nonlinear solution is found, as in the previous section, using PV conservation and geostrophy in each layer and assuming a rigid lid, leading to a second-order ODE for the lower-layer depth:

$$h_{2yy} - \frac{f^2}{g'}\left(\frac{H_{2,k} + H_{1,k}}{H_{2,k}\cdot H_{1,k}}\right)h_2 + \frac{f^2}{g'}\frac{H}{H_{1,k}} = 0 \tag{12}$$

with k denoting the side of the PV front (1 is south) and H the total depth. Solving (12), denoting the locations of the PV fronts in each layer by y_j with the boundary condition that $h_2(\pm\infty) = H_{2k}$ (we assume without loss of generality that $H_{21} > H_{22}$) we find for the lower-layer height:

$$h_2 = \begin{cases} H_{21} + A_1 e^{(y-y_2)/\lambda_1}, & y < y_1 \quad \lambda_1 \equiv \sqrt{g'H_{11}H_{21}/H}/f \\ H_{21} + A_2 e^{(y-y_2)/\lambda_2} + B_2 e^{-(y-y_2)/\lambda_2}, & y_1 < y < y_2 \quad \lambda_2 \equiv \sqrt{g'H_{12}H_{21}/(H_{12} + H_{21})}/f \\ H_{22} + B_3 e^{-(y-y_2)/\lambda_3}, & y_2 < y \quad \lambda_3 \equiv \sqrt{g'H_{12}H_{22}/H}/f, \end{cases} \tag{13}$$

while the lower-layer velocity is found using PV conservation in the lower layer.

Continuous velocities and layer depth and mass conservation result in six nonlinear equations in the unknowns (A_1, A_2, B_2, B_3, y_1, and y_2). This set of equations is solved using a standard root-finding algorithm (all of the numerical analysis in this paper were done using the algorithms in Press et al. 1992). For the case of a surface intersecting front ($H = H_{21}$), where the upper-layer depth vanishes, the boundary conditions are that h_1 and u_2 both vanish at y_1.

The height and velocity profiles in each layer resemble the one found for the 1½-layer model above (with opposite velocities in each layer, shifts of the PV fronts and asymmetries). Unlike the linear solution, the nonlinear solution has a zonally confined along front barotropic transport associated with it.

The energies for the linear problem are given by

$$\text{KE}_{\text{layer1}} = \frac{H_2}{H}G, \quad \text{KE}_{\text{layer2}} = \frac{H_1}{H}G, \quad \Delta\text{PE} = 3G, \tag{14}$$

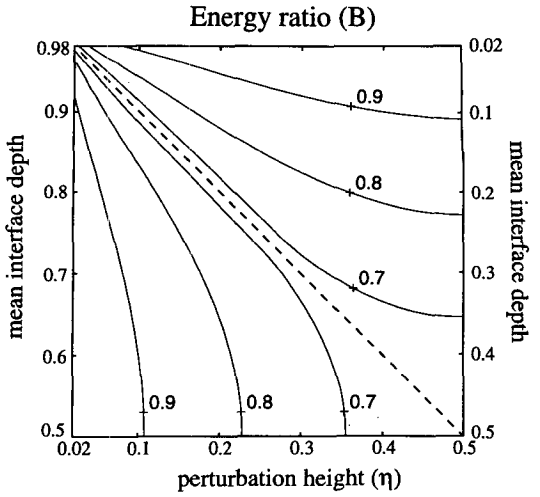

FIG. 2. Energy ratio ($B \equiv \mathrm{KE}_{\mathrm{nonlinear}}/\mathrm{KE}_{\mathrm{linear}} = \Delta\mathrm{PE}_{\mathrm{nonlinear}}/\Delta\mathrm{PE}_{\mathrm{linear}}$) as a function of the interface mean depth ($\bar{H}$) and the perturbation-height (η), both scaled by the total fluid depth H. The broken line divides the figure into $\bar{H} \geq 0.5$ (lower left side) and $\bar{H} \leq 0.5$ (upper right side). By symmetry the energy ratio is the same for $\bar{H}$ and $1 - \bar{H}$.

where

$$G \equiv \frac{\rho g' \lambda \eta^2}{2}, \quad H_j \equiv \frac{H_{j1} + H_{j2}}{2}, \quad \hat{H} \equiv \frac{H_1 H_2}{H_{11} + H_{21}},$$

$$\lambda \equiv \frac{\sqrt{g'\hat{H}}}{f}, \quad \text{and} \quad \eta \equiv \frac{|H_{21} - H_{22}|}{2}.$$

For a given initial perturbation height (η), the KE in each layer increases as the layer depth decreases.

As in the 1 1/2-layer solution, for both linear and nonlinear solutions the ratio of total KE to ΔPE is 1/3. Both the total KE and ΔPE of nonlinear adjustment are less than that for linear adjustment (Fig. 2), with (11) still holding. Here B ($\equiv \mathrm{KE}_{\mathrm{nonlinear}}/\mathrm{KE}_{\mathrm{linear}} = \Delta\mathrm{PE}_{\mathrm{nonlinear}}/\Delta\mathrm{PE}_{\mathrm{linear}}$) decreases more rapidly with increasing perturbation height (η) when the mean depth of the interface ($\bar{H}$, see Fig. 1) is close to the upper or lower boundary. The nonlinear KE can be as small as 40% of the linear value, a much larger difference than the mere few percent in the 1 1/2-layer model. The linear solution is no longer a good approximation when η becomes larger (B less than 90% for $\eta = 0.1$) and when the mean interface between the layers is close to the top or the bottom of the fluid. The energy ratio can be explained as the result of the different Rossby radius of the linear and nonlinear jets near the fronts as in section 2.

3. Adjustment of an axisymmetric "top hat"

We now turn our attention to an axisymmetric configuration in which an additional nonlinearity is present due to the flow curvature. The final state is in cyclogeostrophic rather than geostrophic balance. For the analysis we use a Lagrangian method first introduced by Rossby (1937). We prefer this method over the Eulerian approach used above because mass conservation appears in the form of a differential rather than integral equation. The approach used is similar to the one in Killworth (1992). The 1 1/2-layer (Fig. 3 with $h_1 \to \infty$) shallow-water equations of motion in cylindrical coordinates are

$$\frac{dv_r}{dt} - \frac{v_\theta^2}{r} - fv_\theta = -g\frac{\partial h_2}{\partial r} \tag{15}$$

$$\frac{dv_\theta}{dt} + \frac{v_r v_\theta}{r} + fv_r = 0, \tag{16}$$

where v_r denotes the radial and v_θ the azimuthal velocity. The Lagrangian mass conservation is given by

$$h_2 r dr = H_2 r_{i,2} dr_{i,2}, \tag{17}$$

with $r_{i,2}$ denoting the initial position of the fluid parcel and H_2 its initial height. The angular momentum conservation equation is by (16) (dropping the subscript 2):

$$\frac{d}{dt}\left(rv_\theta + \frac{fr^2}{2}\right) = 0. \tag{18}$$

We integrate (18) to obtain v_θ and together with dh/dr (17), nondimensionalization of depth with the mean depth $\bar{H} \equiv (H_{21} + H_{22})/2$, of the horizontal length scale with $\lambda = \sqrt{g\bar{H}}/f$, and of time with f, (16) gives

$$\frac{d^2 r_i}{dr^2} = \frac{1}{r_i H}\left\{\frac{r^2}{4}\left[\left(\frac{r_i}{r}\right)^4 - 1\right] - r_i \frac{dH}{dr_i}\left(\frac{dr_i}{dr}\right)^2\right\} - \frac{1}{r_i}\left(\frac{dr_i}{dr}\right)^2 + \frac{1}{r}\frac{dr_i}{dr}. \tag{19}$$

The second term on the rhs drops out for our choice of initial conditions (Fig. 3) and (19) is integrated on

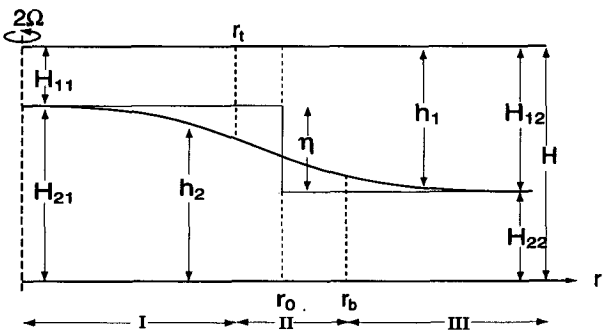

FIG. 3. Schematic for the adjustment of a two-layer axisymmetric perturbation. The initial state (thin line) and the adjusted state (solid line): r_t and r_b denote the new location of the PV front (broken line) in the upper and lower layers (both were initially at r_0). The domain is divided into three region according to the PV distribution in both layers. The mean depth is H_{12} and the initial perturbation height is η. Notice that for both layers the PV front moves towards the shallower water.

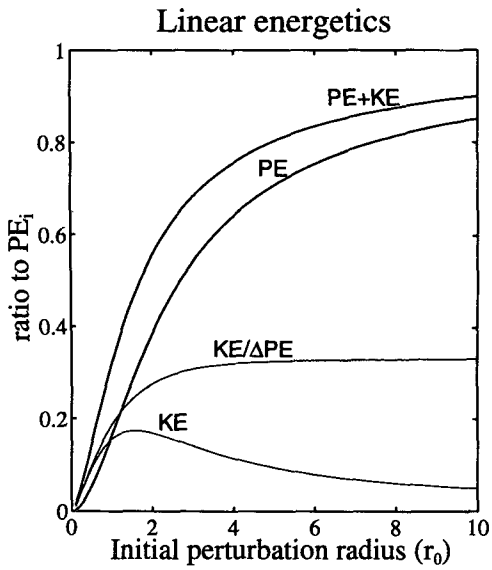

FIG. 4. Energetics of the linear axisymmetric 1 1/2-layer adjustment model. The energies are scaled by the initial potential energy $PE_i = \pi\rho g'\eta^2 r_0^2/2$ and are given as function of the initial perturbation radius (r_0) scaled by $\lambda = \sqrt{g'\bar{H}}/f$.

both sides of the PV front. The boundary conditions are $r_i(r = 0) = 0$, r_i is continuous everywhere, dr_i/dr has a jump given by (18) at r_0, and $r_i = r$ at infinity. Notice that $r(r_0)$ is not known a priori and that, at the origin, (19) is singular, and so we expanded the solution there. Here $r(r_0)$ is found using a numerical integrator combined with a root finder, similar to Killworth's (1992) approach.

The linear solution was found by HO. The normalized (by the initial PE) potential and kinetic energies as function of the initial perturbation radius (r_0) are presented in Fig. 4 (see Middleton 1987 for a detailed explanation of the linear energy profiles).

The ratio of nonlinear to linear energies is shown in Fig. 5. This ratio is different for the PE and KE. As with the geostrophic adjustment, for the cyclogeostrophic adjustment positive (negative) initial perturbations are associated with anticyclonic (cyclonic) adjusted circulation. The KE ratio exceeds unity for wide and positive ($r_0 > 2$, $\eta > 0$) or narrow and negative initial perturbations ($r_0 < 1.5$, $\eta < 0$). It is less than unity for all other cases. The PE ratio is less than one for positive η and larger than one for negative η. The total energy ratio has a similar distribution to the PE ratio for $r_0 > 0.4$ and is therefore not shown.

Two effects determine the observed ratios: the PV front shift of the nonlinear solution and the depth used in the KE calculation. The shift is outward (inward) for positive (negative) initial anomaly, increasing with the anomaly's radius (Fig. 5c). Thus, in the nonlinear solution the height anomaly will spread further out (in) than the linear solution for a positive (negative) anomaly, which results in a smaller (larger) than unity PE ratio. Due to the shift, the linear solution will have larger (smaller) angular velocities for positive (negative) height anomalies thus resulting (since by mass conservation the average height is the same in both solutions) in a smaller (larger) than unity KE ratio. However, as r_0 becomes large compared to the Rossby radius, the height and velocity fields of nonlinear and linear adjustment become similar. Since, in the nonlinear case the total height is used when computing the KE ($KE_{nonlinear} \propto \int hv^2 rdr$) while, in the linear case, the average height ($\bar{H} = H_{22}$) is used ($KE_{linear} \propto \bar{H} \int v^2 rdr$), the KE ratio will change as $h/\bar{H}$, being smaller (larger) than unity for negative (positive) perturbations. When the same analysis was

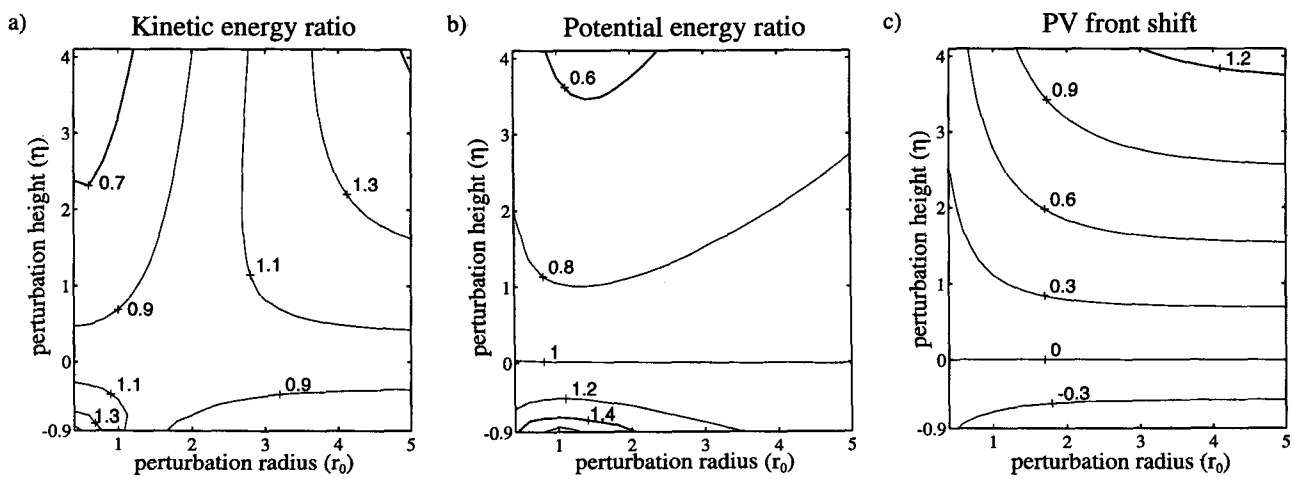

FIG. 5. Energy ratio between the nonlinear and linear solutions and the potential vorticity front shift for the nonlinear solution: (a) contours of KE ratio, (b) PE ratio, and (c) PV front shift (scaled by $\lambda = \sqrt{g'\bar{H}}/f$). All are contoured as a function of the perturbation height η (scaled by $\bar{H}$), and the initial perturbation radius r_0 (scaled by λ).

performed for a finite, zonally uniform perturbation, adjusting geostrophically (rather than cyclogeostrophically) a similar energy ratio was found, indicating that one does not need to invoke cyclogeostrophy to explain the energetics. Killworth's (1992) model is a special case of the above model and can be recovered in the limit of $\eta \gg 1$.

Notice that in the linear adjustment, since PV is conserved locally while mass globally, fluid from the deep side (with low PV) is transfered to the shallow side (with high PV) increasing the amount of fluid with high PV.

4. The intersecting front solution, a model of a convective chimney

Observations of penetrative convection (Anati and Stommel 1970; Gascard 1978; Leaman and Schott 1991) indicate that the bottom layer (or a deep intermediate layer) reaches all the way to the surface during the mixing phase. A geostrophically adjusted solution (Fig. 6) is the simplest representation of the initial collapse of a convective chimney that retains essential features of the dynamics. The solution also supplies an estimate for the amount of energy that radiates away during the initial geostrophic adjustment (eventually the chimney may break up due to baroclinic instability).

A general equation for 2-layer axisymmetric adjustment model is derived in the appendix. The chimney model is a special case of this model and therefore will not be derived here. It consists of (A3) and (A4) with $H_{21} = H$ and the additional boundary conditions that $r_1 = r_0$ and $dr_1/dr = 0$ at $r = r_t$ (solving for $r \geqslant r_t$). As expected and observed (Leaman and Schott 1991), the upper layer has a cyclonic circulation, while the lower an anticyclonic circulation. The energetics of the adjusted state (normalized by the initial PE) and the frontal shift are presented in Fig. 7. The normalized KE and PE depend mainly on the normalized initial chimney size and are weak functions of the upper-layer depth, particularly for small perturbations (their absolute value does depend on the upper-layer depth since the initial potential energy is $\mathrm{PE}_i = \pi\rho g'\eta^2 r_0^2/2$). The normalized upper-layer PV front position (Fig. 7c) depends on the perturbation radii while the lower-layer PV front position (Fig. 7d) depends mainly on the depth of the upper layer. This is due to mass conservation of fluid with the chimney's initial PV. The upper-layer fluid extends horizontally to infinity, and thus its normalized shift (by the upper-layer Rossby radius) can be expected to be of order one.

The ratio of KE to PE released asymptotes to 1/3 as the initial radius grows. (It is above 0.3 for $r_0 = 2.1$.) For a chimney of normalized (as above, by λ_1) initial radius of 1, about 50% of the initial energy is lost, while for a chimney twice that size, less than 30% is lost (Fig. 7). Typical chimneys have radii on the order of 1–16 Rossby radii, the smallest observed in the Weddell Sea and the largest in the northwestern Mediterranean (Killworth 1979). Figure 7 also reveals that, the broader the initial perturbation is, the less of its normalized initial PE is lost.

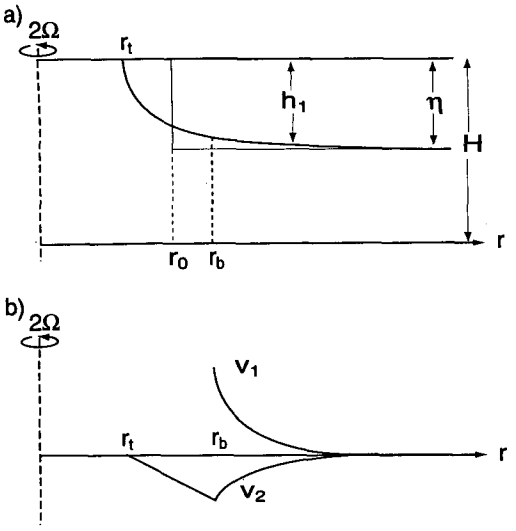

FIG. 6. (a) Schematic for the adjustment of a convective chimney: the initial state (thin line) and the adjusted state (solid line). (b) A representative velocity profile in each layer (in arbitrary units): r_t and r_b denote the new location of the PV front (broken line) in the upper and lower layers (both were initially at r_0). Notice that the circulation is reversed between the layers.

5. Summary and discussion

We have examined solutions for the fully nonlinear, finite Rossby number geostrophic-adjustment problem, in both two-dimensional and axisymmetric geometries. For the 1 1/2-layer zonally uniform step adjustment, the linear solution is an adequate predictor for all values of the initial height jump, but this is not true for the 2-layer step adjustment and for adjustments of perturbations having finite horizontal extent. The agreement found for the step 1 1/2-layer solutions results because the linear and nonlinear models have the same initial height scales with only slightly different Rossby radii. Introduction of a second active layer and/or finite width introduces different Rossby radii for the linear and the nonlinear models. Thus, Middleton's (1987) hypothesis that the linear results will pertain to the nonlinear problems holds only for small initial height perturbations and the 1 1/2-layer zonally uniform step adjustment. However, the ratio of final KE to the PE released during the adjustment is 1/3 for all broad disturbances in both the linear and nonlinear adjustments. In linear adjustments some of the fluid converts from low to high PV, increasing the volume of fluid with high PV. This feature should apply to linear adjustments of mass in a continuously stratified fluid.

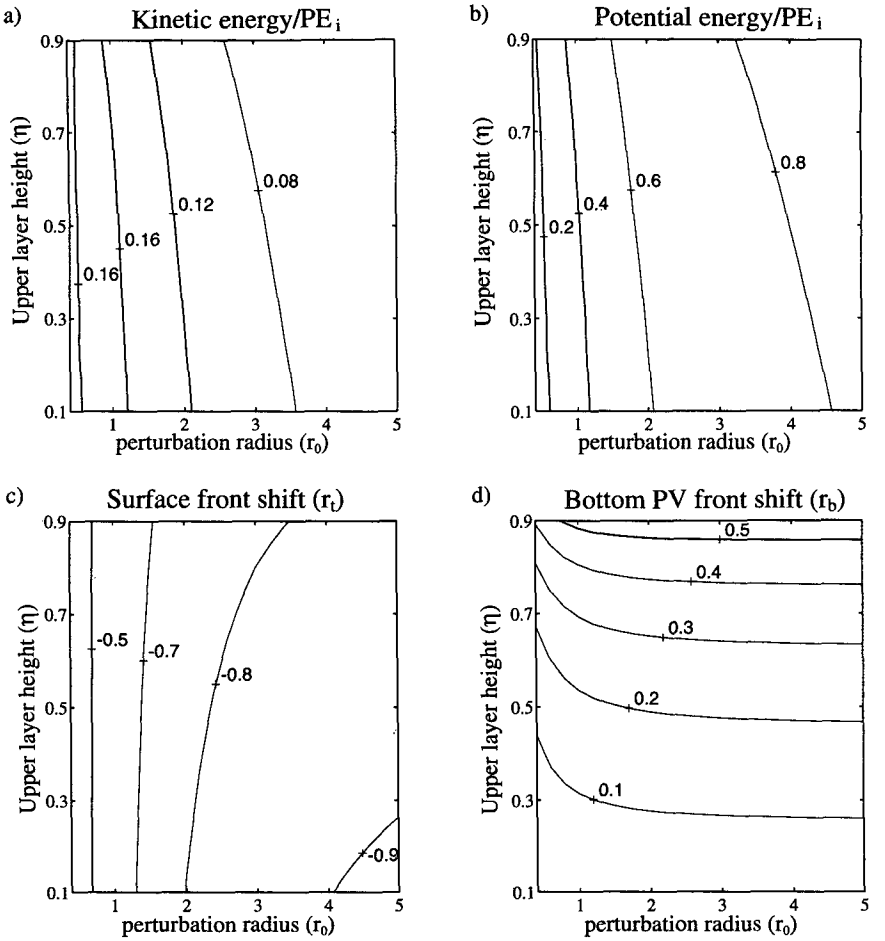

FIG. 7. Energetics and frontal shift for the axisymmetric intersecting front adjustment. The energies are scaled by the initial potential energy $PE_i = \pi\rho g'\eta^2 r_0^2/2$: (a) KE, (b) PE, (c) upper-layer PV front shift, and (d) lower-layer PV front shift. The shifts are scaled by $\lambda_1 = \sqrt{g'\eta}/f$. All are contoured as a function of the perturbation height η (scaled by $\bar{H}$) and the initial perturbation radius r_0 (scaled by λ_1).

A simple 2-layer model was derived to estimate the energy lost during the adjustment of a convective chimney. The energetics (normalized) do not depend strongly on the vertical extent of the upper layer. The dependence on initial radius is very strong for narrow chimneys [found also by McWilliams (1987) for internal eddies].

To determine if it is possible to reach the steady-state solutions described above, it would be necessary to study the transient development of the system. We know that the nonrotating nonlinear infinite-step problem contains a hydraulic jump (Kevorkian 1989, p. 421). If one exists in the rotating solution, it will alter our assumptions about conservation of angular momentum and potential vorticity, thus affecting the energetics. However, the transient linear solution (Gill 1982; HO) does not have a hydraulic jump. Houghton (1969) found that formation of hydraulic jumps is delayed in rotating fluids. If this is the case, then diabatic effects will occur away from the potential vorticity front (since the wave front will have enough time to disperse) and will dissipate energy without affecting the finite region of PV anomaly. Killworth's (1992) investigation of the time-dependent cylinder collapse supports the assumption that the final state is well approximated by the method used in this paper. Another caveat may be that some of the released waves stay trapped inside the adjusting region (due to the velocity shear, Kunze 1985), preventing the steady-state formation. The available linear (Gill 1982; HO) and nonlinear (Killworth 1992) time-dependent solutions do not support this scenario.

Both models and observations suggest that the final breakup of a chimney is due to baroclinic instability (Killworth 1979, Gascard 1978, and HO, to name a few). The timescale of such an instability in the ocean is on the order of 5–10 days. For a 2-layer system undergoing geostrophic adjustment the maximum growth

rate is $f\eta/\bar{H}$ (i.e., a timescale of $\bar{H}/f\eta$, HO), with η being the initial perturbation height and $\bar{H}$ the average layer depth. The geostrophic adjustment timescale for a chimney of horizontal extent L and internal depth H is $\tau_a = L^2 f/\pi g' H$ (HO; Middleton 1987). For a chimney of horizontal extent $L = \alpha \cdot \lambda$ (λ, the internal Rossby radius), the timescale reduces to $\tau_a = \alpha^2/\pi f$. The ratio between the geostrophic adjustment to the instability timescale is therefore $\alpha^2\eta/\pi\bar{H}$. Narrow chimneys with small vertical extent can therefore adjust before instability develops, and since they radiate energy, the instability's growth can be considerably slowed. Broader and taller chimneys will take longer to adjust, having large-amplitude internal waves that propagate slowly (HO; Saint-Gully 1972). These chimneys will become baroclinically unstable long before they adjust geostrophically. Barotropic shear instability may be expected for chimneys that are narrow and tall due to their adjusted high velocity shear (which can be inferred here from their high KE). The growth rate of barotropic instability is proportional to the shear (Gill 1982).

Baroclinic instability is expected in all the two-dimensional configurations presented here, since all have a reversal of PV gradient between the top and bottom layers. The intersecting front is a special case of the 2-layer configuration and is thus expected to become unstable too.

Acknowledgments. We wish to thank E. Kunze for first interesting us in geostrophic adjustments. Discussions with M. Kawase and A. Hermann were useful and stimulating. Comments made by C. Lee, J. Dairiki, and D. Codiga are appreciated. EB was supported by the University of Washington Graduate School Fund and LT by a Office of Naval Research Young Investigator Award.

APPENDIX

Two-Layer Axisymmetric Model

For a 2-layer axisymmetric disturbance (Fig. 3), the derivation is similar to that of Dewar and Killworth (1990). However, where they find a linear ODE, we get a nonlinear one. Dewar and Killworth's (1990) configuration is a special case of the one presented here. Combining the 2-layer azimuthal momentum equations in steady state gives

$$\frac{v_1^2 - v_2^2}{r} + f(v_1 - v_2) = g' \frac{dh_1}{dr}, \qquad \text{(A1)}$$

where subscripts denote layer (1 being top) and v is the azimuthal velocity. Angular momentum conservation implies

$$rv_j + \frac{fr^2}{2} = \frac{fr_{i,j}^2}{2}, \quad j = 1, 2, \qquad \text{(A2)}$$

where r_i is the initial position of the particle (column of fluid) and j is the layer in which it resides. We use the following notation, after Dewar and Killworth (1990):

$$P_1 \equiv \frac{r_{i,1}^2}{2}, \quad P_2 \equiv \frac{r_{i,2}^2}{2}, \quad P_0 \equiv \frac{r_0^2}{2},$$

$$q \equiv \frac{r^2}{2}, \quad q_t \equiv \frac{r_t^2}{2}, \quad q_b \equiv \frac{r_b^2}{2}.$$

Using these relations with (A1), (A2) and mass conservation (17) in the upper layer,

$$\frac{g'H_{1k}}{f^2}\frac{d^2P_1}{dq^2} = \frac{1}{4q^2}[(P_1 - q)^2 - (P_2 - q)^2] + \frac{1}{2q}(P_1 - P_2). \qquad \text{(A3)}$$

The domain is divided into three distinct regions (Fig. 3). The extent of region II will be determined by whether the anomaly is positive ($q_t < q_b$) or negative ($q_t > q_b$). We will assume a positive anomaly ($H_{21} > H_{22}$); the derivation is similar for a negative one. We solve for P_2 in each of the three regions by integrating the corresponding Lagrangian mass equation ($H_{ik}dP_i/dq = h_i$), adding them and matching at the PV boundary,

$$\begin{aligned} &q < q_t: && H_{21}P_2 = Hq - H_{11}P_1 \\ &q_t < q < q_b: && H_{21}P_2 = Hq - H_{12}P_1 + (H_{12} - H_{11})P_0, \\ &q_b < q: && H_{22}P_2 = Hq - H_{12}P_1 \end{aligned} \qquad \text{(A4)}$$

where H is the total depth. Substituting (A4) into (A3) gives a second-order ODE for P_1 in each region. A priori q_t and q_b are not known but can be found numerically using the following boundary conditions:

$$\begin{aligned} &\text{at } q = 0, && P_1 = 0 \\ &\text{at } q = q_t, && P_1(q_t^-) = P_1(q_t^+) \text{ and } \frac{dP_1}{dq_{q_t^-}} = \frac{H_{12}}{H_{11}}\frac{dP_1}{dq_{q_t^+}} \\ &\text{at } q = q_b, && P_1(q_b^-) = P_1(q_b^+) \text{ and } \frac{dP_1}{dq_{q_b^-}} = \frac{dP_1}{dq_{q_b^+}} \\ &\text{at } q \to \infty, && \frac{dp_1}{dq} \to 1. \end{aligned} \qquad \text{(A5)}$$

Since we solve a second-order ODE, we need only one boundary condition at each end. The two additional boundary conditions are used to determine the position of q_t and q_b. Dewar and Killworth's (1990) case is recovered taking $H_{12} = H_{21} = H$.

REFERENCES

Anati, D., and H. Stommel, 1970: The initial phase of deep water formation in the northwest Mediterranean, during MEDOC

'69, on the basis of observations made by "Atlantis II" January 25–February 12, 1969. *Cah. Oceanogr.*, **22,** 343–351.

Blumen, W., 1967: On nonlinear geostrophic adjustment. *J. Atmos. Sci.*, **24,** 325–332.

——, 1972: Geostrophic adjustment. *Rev. Geophys. Space Phys.*, **10,** 485–528.

Dewar, W. K., and P. D. Killworth, 1990: On the cylinder collapse problem, mixing, and the merger of isolated eddies. *J. Phys. Oceanogr.*, **20,** 1563–1575.

Gascard, J.-C., 1978: Mediterranean deep water formation, baroclinic instability and oceanic eddies. *Oceanol. Acta.*, **1,** 315–330.

Gill, A. E., 1976: Adjustment under gravity in a rotating channel. *J. Fluid Mech.*, **77,** 603–621.

——, 1982: *Atmosphere-Ocean Dynamics,* Academic Press, 662 pp.

Hermann, A. J., and W. B. Owens, 1993: Energetics of gravitational adjustment in mesoscale chimneys. *J. Phys. Oceanogr.*, **23,** 346–371.

Houghton, D. D., 1969: Effect of rotation on the formation of hydraulic jumps. *J. Geophys. Res.*, **74,** 1351–1360.

Kevorkian, J., 1989: *Partial Differential Equations.* Wadsworth & Brooks/Cole Advanced Books & Software, 547 pp.

Killworth, P. D., 1979: On "chimney" formations in the ocean. *J. Phys. Oceanogr.*, **9,** 531–554.

——, 1992: The time-dependent collapse of a rotating fluid cylinder. *J. Phys. Oceanogr.*, **22,** 390–397.

Kunze, E., 1985: Near-inertial wave propagation in geostrophic shear. Ph.D thesis, University of Washington, 90 pp.

Leaman, K. D., and F. A. Schott, 1991: Hydrographic structure of the convection regime in the Gulf of Lions: Winter 1987. *J. Phys. Oceanogr.*, **21,** 575–598.

McWilliams, J. C., 1988: Vortex generation through balanced adjustment. *J. Phys. Oceanogr.*, **18,** 1178–1192.

Middleton, J. F., 1987: Energetics of linear geostrophic adjustment. *J. Phys. Oceanogr.*, **17,** 735–740.

Ou, H. W., 1984: Geostrophic adjustment model of a tidal mixing front. *J. Phys. Oceanogr.*, **14,** 994–1000.

Press, W. H., S. A. Teukolsky, W. T. Vetterling, and B. P. Flannery, 1992: *Numerical Recipes in C.* Cambridge University Press, 994 pp.

Rossby, C. G., 1937: On the mutual adjustment of pressure and velocity distributions in certain simple current systems. I. *J. Mar. Res.*, **1,** 15–28.

Saint-Guily, B., 1972: On the response of the ocean to impulse. *Tellus,* **24**(4), 344–349.

van Heijst, G. J. F., 1985: A geostrophic adjustment model of a tidal mixing front. *J. Phys. Oceanogr.*, **15,** 1182–1190.